J Neurophysiol 102: 636–643, 2009.
First published April 22, 2009; doi:10.1152/jn.00012.2009.

Reverse Optical Trawling for Synaptic Connections In Situ

Takuya Sasaki,[1] Genki Minamisawa,[1] Naoya Takahashi,[1] Norio Matsuki,[1] and Yuji Ikegaya[1,2]
[1]*Laboratory of Chemical Pharmacology, Graduate School of Pharmaceutical Sciences, The University of Tokyo; and* [2]*Precursory Research for Embryonic Science and Technology, Japan Science and Technology Agency, Tokyo, Japan*

Submitted 6 January 2009; accepted in final form 19 April 2009

Sasaki T, Minamisawa G, Takahashi N, Matsuki N, Ikegaya Y. Reverse optical trawling for synaptic connections in situ. *J Neurophysiol* 102: 636–643, 2009. First published April 22, 2009; doi:10.1152/jn.00012.2009. We introduce a new method to unveil the network connectivity among dozens of neurons in brain slice preparations. While synaptic inputs were whole cell recorded from given postsynaptic neurons, the spatiotemporal firing patterns of presynaptic neuron candidates were monitored en masse with functional multineuron calcium imaging, an optical technique that records action potential–evoked somatic calcium transients with single-cell resolution. By statistically screening the neurons that exhibited calcium transients immediately before the postsynaptic inputs, we identified the presynaptic cells that made synaptic connections onto the patch-clamped neurons. To enhance the detection power, we devised the following points: *1*) $[K^+]_e$ was lowered and $[Ca^{2+}]_e$ and $[Mg^{2+}]_e$ were elevated, to reduce background synaptic activity and minimize the failure rate of synaptic transmission; and *2*) a small fraction of presynaptic neurons was specifically activated by glutamate applied iontophoretically through a glass pipette that was moved to survey the presynaptic network of interest ("trawling"). Then we could theoretically detect 96% of presynaptic neurons activated in the imaged regions with a 1% false-positive error rate. This on-line probing technique would be a promising tool in the study of the wiring topography of neuronal circuits.

INTRODUCTION

Neural circuits are composed of myriads of synapses, which are believed to be important sites for information processing and storage. However, little is known about their wiring structure and the unitary properties of individual synapses, mainly because there have not been any available techniques to search single synaptic connections in living brain tissues. Detection of synaptically connected neuron pairs has usually been achieved by random selection of two neurons; however, this is stochastically inefficient, given that the connection densities of excitatory synapses are only 10–20% between even neighboring neurons in the neocortex (Feldmeyer et al. 2005; Le Bé and Markram 2006; Song et al. 2005) and about 10% between hippocampal CA3 and CA1 regions (Bolshakov and Siegelbaum 1995; Sayer et al. 1990).

We describe a new method, termed reverse optical "trawling" (ROTing), to functionally scan synaptic connectivity in brain slice preparations with the help of whole cell patch-clamp recording and functional multineuron calcium imaging (fMCI), a technique that optically monitors many neurons in situ and detects their action potentials as the resulting "calcium transient" events in their somata (Takahashi et al. 2007). The technical concept of ROTing originates from a reverse optical "probing" (ROPing) technique introduced by Aaron and Yuste (2006). The experimental idea is that, if neuron A repeatedly shows calcium events that are time-locked to postsynaptic currents (PSCs) recorded in neuron B, neuron A is a putative presynaptic source of neuron B. Based on this idea, ROPing finds presynaptic neurons by imaging spontaneous firing activity from a local network surrounding the whole cell recorded neurons. Although ROPing operates under certain conditions, its detection power is highly susceptible to the level of background activity that arises from neurons hidden outside of the field of view and, more crucially, ROPing cannot detect synaptic connections unless the presynaptic candidates spontaneously fire action potentials during the probing period.

Our ROTing method overcomes these problems. Background noise activity is minimized by lowering the extracellular K^+ concentration and elevating the divalent ion concentrations. ROTing is also designed to thoroughly search (or "trawl" in) a presynaptic network by activating only a few neurons through local application of glutamate through a movable glass pipette little by little. We report that these procedures improve the signal-to-noise ratio and the detection power of ROTing to a point that can almost completely determine the synaptic projection pattern between a few patch-clamped postsynaptic neurons and dozens of presynaptic neurons imaged in a local circuit.

METHODS

Slice preparation

According to the University of Tokyo guidelines for the care and safety of laboratory animals, hippocampal slice cultures were prepared from postnatal day 7 Wistar/ST rats (SLC, Shizuoka, Japan) as previously described (Koyama et al. 2007). Briefly, rat pups were chilled with ice and decapitated. The brains were removed and horizontally cut into 300-μm-thick slices using a DTK-1500 vibratome (Dosaka, Kyoto, Japan) in aerated, ice-cold Gey's balanced salt solution supplemented with 25 mM glucose. Entorhino-hippocampal stumps were excised and cultivated on Omnipore membrane filters (JHWP02500; Millipore, Bedford, MA) that were laid on plastic O-ring disks. The cultures were fed with 1 ml of 50% minimal essential medium, 25% Hanks' balanced salt solution, 25% horse serum (Cell Culture Laboratory, Cleveland, OH), and antibiotics in a humidified incubator at 37°C in 5% CO_2. The medium was changed every 3.5 days.

For experiments with acute slice preparations, postnatal 10- to 11-day-old ICR mice (SLC) were anesthetized with ether and decapitated. The brain was immersed in ice-cold low-Na^+ artificial cerebrospinal fluid (ACSF) consisting of (in mM) 27 $NaHCO_3$, 1.4 NaH_2PO_4, 2.5 KCl, 0.5 ascorbic acid, 7.0 $MgSO_4$, 1.0 $CaCl_2$, and 222 sucrose, bubbled with 95% O_2-5% CO_2. Horizontal entorhino-hippocampal slices of 400-μm thickness were cut using a vibratome

Address for reprint requests and other correspondence: T. Sasaki, Laboratory of Chemical Pharmacology, Graduate School of Pharmaceutical Sciences, The University of Tokyo, Yokyo 113-0033, Japan (E-mail: ff077204@mail.ecc.u-tokyo.ac.jp).

(Vibratome 3000; Vibratome, St. Louis, MO) and maintained for >60 min at room temperature in normal ACSF consisting of (in mM): 127 NaCl, 26 $NaHCO_3$, 1.6 KCl, 1.24 KH_2PO_4, 1.3 $MgSO_4$, 2.4 $CaCl_2$, and 10 glucose.

Functional multineuron calcium imaging

On days 6–14 in vitro, slices were mounted in a recording chamber at 32°C perfused with modified ACSF consisting of (in mM) 123 NaCl, 26 $NaHCO_3$, 2.2 KCl, 1.24 NaH_2PO_4, 3.0 $MgSO_4$, 3.0–3.2 $CaCl_2$, and 10 glucose, bubbled with 95% O_2-5% CO_2. A glass pipette (1–3 MΩ) for dye loading was filled with ACSF consisting of 200 μM Oregon Green 488 BAPTA-1 acetoxymethyl (OGB-1-AM, Invitrogen), 2% pluronic F-127 (Invitrogen), and 20% DMSO. The tip of the pipette was inserted into the pyramidal cell layer and the dye solution was pressure-ejected for 3–5 min by manually controlling a 10-ml syringe pressurizer (50–60 kPa). After loading the indicator, another glass electrode (~1 MΩ) filled with 10 μM glutamate in ACSF was placed at 20 μm above the surface of the slices. Glutamate was iontophoretically applied by injecting negative rectangular currents of 3–30 μA for 1–5 s through the electrode. The currents were intermittently applied at intervals of 3–5 s to avoid excessive neuronal activation due to extracellular glutamate accumulation.

The fluorophores were excited at the 488-nm line of an argon-krypton laser (5–10 mW, 641-YB-A01; Melles Griot, Carlsbad, CA) and were visualized through a 507-nm-long pass emission filter. Images (512 × 512 pixels = 520 × 520 μm, 14-bit intensity) were captured at 50 frames/s using a Nipkow-disk confocal scanner unit (CSU-X1; Yokogawa Electric, Tokyo, Japan), a cooled CCD camera (iXON DV897; Andor, Belfast, Northern Ireland, UK), an upright microscope (Eclipse FN1; Nikon, Tokyo, Japan), and a water-immersion objective (×16, 0.8 NA, CFI75LWD16XW, Nikon).

For extracting spike activity, the cell bodies of neurons were identified by eye to define the regions of interest (10-μm-radius circles). The fluorescence intensity was averaged in space in these regions. For each cell, the change in the fluorescence ($\Delta F/F$) was calculated as $(F_t - F_0)/F_0$, where F_t is the fluorescence intensity at any time point, and F_0 is the average baseline fluorescence intensity across the 10-s periods before and after the focused time point. This normalization was used to compensate photobleaching due to long-time imaging (Sasaki et al. 2007). The onsets of the calcium transients were automatically or semiautomatically detected using a Matlab program based on the principal component analysis and support-vector machine (Sasaki et al. 2008).

Electrophysiological recording

Patch-clamp recordings were carried out with a MultiClamp 700B amplifier and a Digidata 1440A digitizer controlled by pCLAMP 10 software (Molecular Devices, Union City, CA). For whole cell recordings, borosilicate glass pipettes (4–9 MΩ) were filled with internal solution consisting of (in mM): 135 K-gluconate, 4 KCl, 10 HEPES, 10 phosphocreatine-Na_2, 0.3 Na_2-GTP, and 4 Mg-ATP (pH 7.2). For perforated patch-clamp recordings, amphotericin B (Sigma–Aldrich, St. Louis, MO) was dissolved in DMSO and then diluted (1:250) to the final concentration of 240 μg/ml in a KCl-based filling solution containing (in mM) 150 KCl, 10 HEPES, and 0.5 EGTA (pH 7.2). The solution was used only within 3 h after preparation. Signals were low-pass filtered at 1–2 kHz, digitized at 10 kHz, and analyzed with pCLAMP 10 software. Excitatory and inhibitory PSCs were isolated by clamping at −70 and 0 mV, respectively. PSCs were automatically extracted with a criterion for the peak current sizes of >5 pA. During glutamate puffs, PSCs that followed within <50 ms after the first PSCs were eliminated because they could be merely events that arose from burst firings by the identical presynaptic neurons. Data were discarded when the average PSC frequency was >5 Hz because high background activity deteriorates the detection power of ROTing (see following text).

Detection of synaptically connected neuron pairs

To statistically determine whether a given neuron pair is synaptically coupled, we calculated the P value, defined as the probability that the observed number of "coincidences" of calcium events in fMCI-monitored neuron$_i$ and PSCs recorded from neuron$_j$ happens by chance in the same level of background PSCs under the assumption that neuron$_i$ and neuron$_j$ are a nonsynaptic pair. The coincidence is defined when a PSC occurs at the movie frame of a calcium event. Because optical noise occasionally causes one-frame detection errors for calcium event timings (Sasaki et al. 2008), one frame jitter was allowed for the coincidence—that is, the time window allowed was 60 ms (=20 ms ×3)—because movies were taken at a frame rate of 50 frames/s. Let f_i and f_j denote the event frequencies of neuron$_i$ and neuron$_j$, respectively. The expected frequency of event coincidence in a random Poisson process is $f_i \times f_j$. Thus if n out of the total N calcium events in neuron$_i$ coincide with PSCs in neuron$_j$, the P value between neuron$_i$ and neuron$_j$ is calculated as

$$p = \sum_{k=n}^{N} {}_N C_k (1 - f_i \times f_j)^{N-k} (f_i \times f_j)^k$$

We consider a synaptic projection from neuron$_i$ to neuron$_j$ when the P value is <0.01.

Data representation

Data are reported as means ± SD.

RESULTS

Experimental procedures of ROTing

We describe ROTing by exemplifying hippocampal CA3-to-CA1 synaptic connections, unless otherwise specified. The experimental scheme is shown in Fig. 1. ROTing consists of three steps as follows:

Step 1. Calcium-sensitive fluorescent indicator is injected into presynaptic CA3 neuron candidates (Fig. 1, Step 1). We chose the local AM-dye-loading method, rather than incubation of slice preparations in AM-dye solution because *1*) time spent for the local loading is shorter than that for bath incubation (Ikegaya et al. 2005) and *2*) loaded indicators might affect synaptic transmission and other biological processes; because the indicators by themselves serve as an intracellular calcium chelator, the loaded area should be as small as possible. We usually used OGB-1-AM, because it reliably reports action potential–evoked calcium transients due to its fast kinetics and high affinity for calcium (K_d = 170 nM) (Takahashi et al. 2007).

For loading, the tip of a glass pipette was inserted into the CA3 stratum pyramidale, and OGB-1-AM was ejected by raising the pipette pressure. Figure 2*A* demonstrates the time course of OGB-1 loading in the CA3 region. Dozens of neurons within a radius of about 200 μm around the pipette tip were labeled after 3–5 min. When the pressure application was further prolonged, the stained area and the number of labeled neurons were almost unchanged, although the fluorescence intensity continued to increase (data not shown). Even after 3–5 min of application, the labeled neurons were already capable of showing evident calcium transients in response to

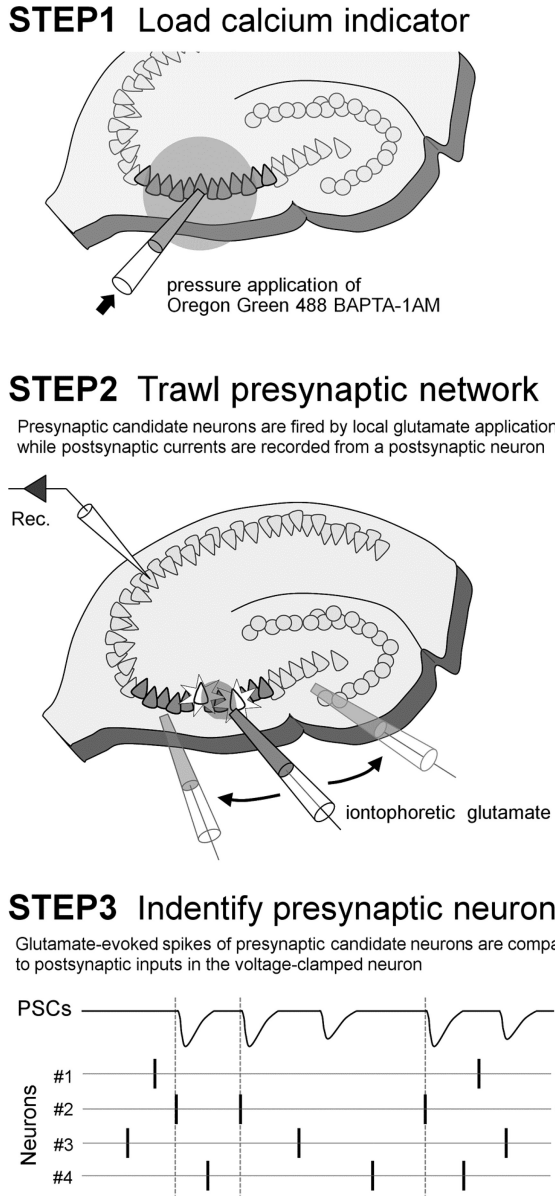

FIG. 1. Schematic illustration for the reverse optical "trawling" (ROTing) procedure: an example of hippocampal CA3–CA1 synaptic mapping. The experimental paradigm consists of 3 steps. Step 1: fluorescent calcium AM-indicator is pressure-injected into a small part of the CA3 region in a hippocampal slice. Step 2: neurons in the dye-loaded region are specifically activated by iontophoretic application of glutamate through a movable glass pipette, and the spatiotemporal pattern of the evoked network activity is monitored with functional multineuron calcium imaging (fMCI), during which period the relevant postsynaptic currents (PSCs) are simultaneously whole cell recorded from a CA1 pyramidal neuron. Step 3: timings of the recorded PSCs are carefully compared relative to the calcium event timings of individual CA3 neurons and presynaptically connected neurons are determined based on their probabilistic saliences. In this case, neuron 2 is a strong candidate.

single spikes (Fig. 2*D*). Thus the 3- to 5-min injection is sufficient for ROTing.

Step 2. The dye-loaded CA3 neurons are fired by iontophoretic application of glutamate and the resultant PSCs are whole cell recorded in a given CA1 neuron (Fig. 1, Step 2). The spatiotemporal firing pattern of CA3 neurons is monitored with fMCI, whereas the PSCs are recorded at a clamped voltage of −70 mV. A glass electrode is placed about 20 μm from the top surface of the slice preparation and glutamate is puffed onto a subset of CA3 neurons by applying a negative current through the electrode. The electrode is manually moved along the pyramidal cell layer at the velocity of 15–30 μm/s, to fully cover the dye-loaded region (Fig. 2*B*). The local application of glutamate usually stimulated <3 neurons within a radius of about 50 μm around the electrode tip and many neurons were sequentially activated along the electrode trajectory (Fig. 2*C*). Figure 2*E* shows the distribution of the frequency of evoked calcium events and the mean event frequency was 1.2 ± 1.0/min (n = 596 neurons). Under these conditions, 91.7% of the loaded neurons were activated at least once for a 5-min period of glutamate application (n = 10 slices).

Simultaneous patch-clamp recording and calcium imaging from the same neurons revealed that calcium events reflected action potentials and that most of the individual events are associated with multiple spikes, i.e., burst firing events (Fig. 2*D*). Figure 2*F* shows the distribution of spike counts in single bursts. The mean spike count was 3.5 ± 1.9 and the mean burst frequency was 11.5 ± 5.6 Hz (n = 327 bursts in 6 cells).

In general, the neuronal networks are spontaneously active. Therefore the patch-clamped neurons receive not only the specific inputs from glutamate-activated presynaptic neurons

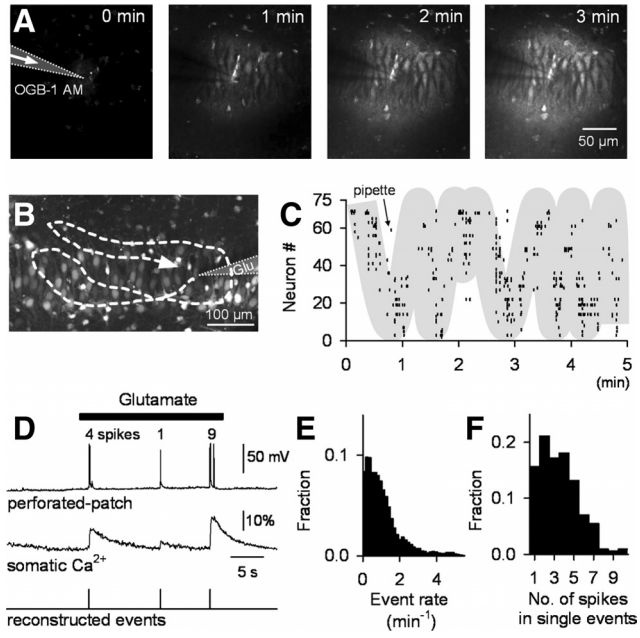

FIG. 2. fMCI of glutamate-evoked neuronal activity. *A*: time-lapse confocal images of injection of 200 μM Oregon Green 488 BAPTA-1 acetoxymethyl (OGB-1-AM) dye into the CA3 stratum pyramidale in a cultured hippocampal slice. *B*: confocal images of the CA3 stratum pyramidale, including many neurons labeled with OGB-1. The white broken line indicates the trajectory along which the tip of a glass pipette used for glutamate iontophoresis moved. *C*: raster plot of the spatiotemporal pattern of calcium events monitored with fMCI. The shaded area represents the activated regions during the pipette movement. *D*: simultaneous perforated patch-recording (*top*) and somatic calcium signal sampled at a frame rate of 50 Hz (*middle*) from a neuron that received local application of glutamate during the period indicated by the black bar. Glutamate often evoked burstlike events of action potentials. The number of spikes involved in each event is indicated above the *top trace*. The *bottom line* indicates the reconstructed timings of calcium transients. *E*: distribution of the frequency of calcium events evoked in individual neurons. Data were collected from 596 CA3 neurons (n = 10 slices). *F*: distribution of the number of action potentials in single events.

but also ongoing synaptic inputs from the surrounding network. The background activity decreases the detection power of ROTing because the spontaneous activity increases the chance coincidence of calcium events and PSCs. To reduce the background activity, we modified the ionic compositions of ACSF, that is, the K^+ concentration was lowered to 2.2 mM, whereas the Ca^{2+} and Mg^{2+} concentrations were increased to 3.0–3.2 and 3.0 mM, respectively. In the modified solution, the mean frequencies of spontaneous PSCs were 2.2 ± 1.6 Hz (n = 8 neurons) and 2.6 ± 1.3 Hz (n = 8 neurons) without and during glutamate application, respectively, whereas it was 63.7 ± 12.7 Hz (n = 10 neurons) in low-Ca^{2+}/high-K^+ ACSF solution (4.5 mM K^+, 1.2 mM Ca^{2+}, 2.0 mM Mg^{2+}) introduced by Sanchez-Vives and McCormick (2000). Likewise, the mean frequency of spontaneous calcium events was 0.0013 ± 0.0002/min (n = 458 neurons from 10 slices) in the modified solution, whereas it was 5.3 ± 2.7/min (n = 501 neurons) in the low-Ca^{2+}/high-K^+ ACSF.

Another advantage of the modified ACSF is that higher Ca^{2+} concentrations increase the synaptic release probability of CA3 neurons (Pavlidis and Madison 1999). This contributes to reduce the false-negative error rate of ROTing (see following text). In the modified solution, the mean transmission probability of CA3-to-CA1 synapses was 90.1 ± 11.4%, the median being 93% (n = 52 pairs from 35 slices; see also Fig. 4*C*).

Step 3. By comparing the relative timing between presynaptic calcium events and PSCs, all neuron pairs are evaluated as to whether they are synaptically connected (Fig. 1, Step 3). An example is shown in Fig. 3. For every presynaptic candidate, we calculated the P value, an index of the significant coincidence of calcium events and PSCs, i.e., the probability that the observed number of the coincidence takes place in a given frequency of background PSCs if they are synaptically uncoupled and behave as independent Poissonian units (see METHODS). Figure 3*A* shows representative calcium events of eight CA3 neurons and synaptic activity in a patched CA1 cell. As the glutamate pipette moved in the direction from neuron 1 to neuron 8, single or a few neurons were sequentially activated around the pipette tip.

In most cases, glutamate-evoked calcium events involved multiple spikes (Fig. 2*F*). When a barrage of PSCs at interevent intervals of <50 ms was observed in the patched neuron, only the first PSC was thus considered in ROTing and the subsequent PSCs were ignored because they could be PSCs elicited by the same presynaptic neurons. This procedure is also important from a technical perspective because individual presynaptic spikes in a high-frequency burst were inseparable in the calcium event due to its slow calcium decay kinetics (Sasaki et al. 2008).

In the example data, the P value of neuron 4 was lower than a threshold of 0.01 and this statistical salience indicates that there is likely a synaptic connection between the patched and imaged neurons. Indeed, the superimposition of 10 consecutive patch-clamp traces aligned to the timings of calcium events in neuron 4 revealed that PSCs occurred frequently coincident with the calcium events (Fig. 3*B*). Then, we targeted the putative presynaptic neuron for the whole cell configuration. As expected, the single spikes triggered in this neuron were followed by PSCs in the previously patched CA1 neuron (Fig. 3*C*).

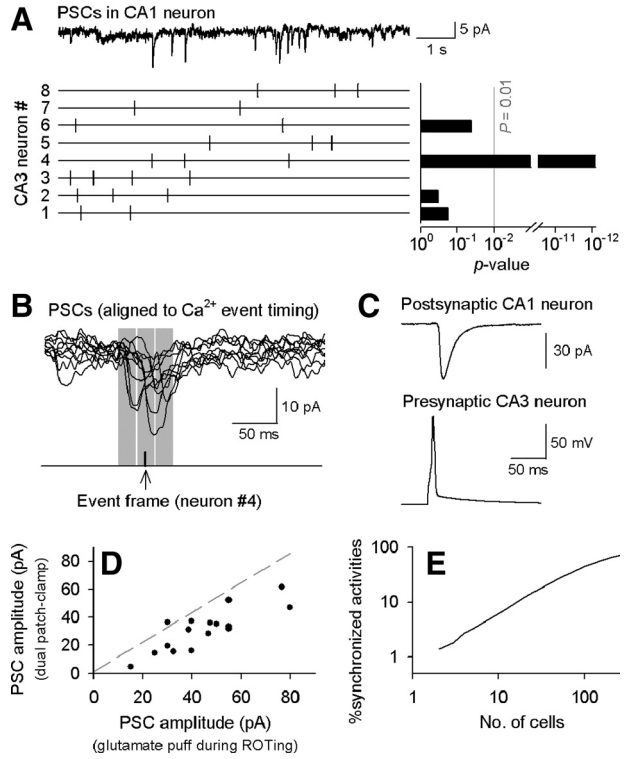

FIG. 3. ROTing for synaptically connected neurons in hippocampal slices. *A*: the spatiotemporal firing pattern of 8 CA3 neurons in response to local application of glutamate was monitored with fMCI (*bottom left*), whereas PSCs were simultaneously recorded from a CA1 pyramidal neuron (*top left*). The data shown here are a part of long-term recording. The *right histogram* shows the P values of individual neurons. The P value indicates the significance level of coincidence of calcium events and PSCs. In this case, neuron 4 exhibited a P value lower than a threshold of 0.01. *B*: 10 consecutive traces of postsynaptic currents were aligned to each calcium event onset of neuron 4. The shaded areas represent 3 imaging frames around the calcium events. *C*: double recordings from monosynaptically coupled neurons. Single spikes elicited in a CA3 presynaptic neuron identified with ROTing gave rise to monosynaptic excitatory PSCs in the CA1 postsynaptic neuron. Traces were averaged across 50 consecutive trials of current injection (1.2 nA, 5 ms). The mean latency from the presynaptic spike to the PSC onset was 4.3 ± 0.6 ms, suggestive of monosynaptic transmission. *D*: relationship between PSCs evoked by glutamate puffs during ROTing and single presynaptic spikes during subsequent patch-clamp recordings (R = 0.83, n = 16 cell pairs from 7 slices). Each dot indicates the data of a single cell pair. Broken line indicates the direct proportion with the slope of 1. *E*: percentage of synchronized calcium events to the total events in a glutamate-activated local network: a numerical simulation. The percentage increases with the number of cells activated by glutamate.

For each pair, the amplitude of single spike-evoked PSCs monitored by dual patch-clamp recordings was compared with that evoked by glutamate puffs during ROTing (Fig. 3*D*). These PSCs were positively correlated (R = 0.84, $P < 0.001$), indicating that ROTing not only predicts the existence of synaptic connections but can also roughly estimate their functional strength. The glutamate-versus-spike regression slope was <1, that is, the PSCs during ROTing were larger values than those by dual recordings. This is presumably because glutamate puff evoked burst firings of presynaptic neurons and thus PSCs are summed or the failure of synaptic transmission was reduced.

The mean event frequencies of cells located in glutamate puffed areas were about 0.3 Hz. This value was higher than the mean activity rate during the entire time period of ROTing (see

Fig. 2*E*). For example, the raster plot in Fig. 3*A* represents the time period during which the glutamate pipette was moving above these neurons; note the neurons were briefly activated during the period shown here, but otherwise mostly silent. When neurons exhibit calcium events at such high frequencies, the chance of activity coincidence increases; thus it is difficult to identify the presynaptic neurons responsible for the observed PSCs. To estimate the chance level, we computed the ratio of coincident activity by assuming that neurons behave as independent Poissonian units with the mean event frequency of 0.3 Hz (Fig. 3*E*). The coincidence was defined when a cell pair generated the activity within the time window of 60 ms (i.e., three frames of 50-Hz imaging). As expected, the percentages of calcium events that were coincident with any event of another neuron to the total number of glutamate-evoked events increased as a function of the number of cells considered. Given that <3 neurons were usually activated by our local glutamate application procedure, the majority (>98%) of the events were not synchronized, being temporally separable enough to compare PSC events. In addition, this simulation implies that the number of cells evoked by glutamate puffs must be lowered as few as possible (practically <10 cells), to isolate the responsible presynaptic neurons.

Statistical validation of ROTing

The detection power of ROTing depends on how many calcium events are evoked in the postsynaptic neuron candidates. If only few calcium events are used for the *P* value calculation, the detection loses reliability. To determine the minimal number of calcium events required for practically precise detection, we simulated the detection power of ROTing as a function of the number of presynaptic events to be considered.

For this purpose, we performed dual recordings from monosynaptically connected neurons ($n = 8$ pairs). In the presence of background PSCs in the modified ACSF, PSCs were recorded for about 10 min, during which period presynaptic neurons were fired by brief current injection at 0.5–1.0 Hz. Note that, under these conditions, PSCs do not always follow the presynaptic spikes because of occasional failures of synaptic transmission and also that PSCs happen to appear even at failure transmission trials because of spontaneous network activity. Using these real data sets, we estimated the false-negative errors, i.e., errors in which presynaptically connected neurons were judged as unconnected ones (Fig. 4*A*). Trial series of success and failure transmissions were collected from these data sets, a given number of the trials were randomly selected, and the *P* values were calculated by taking the background PSC frequency into consideration. The *left plot* in Fig. 4*A* depicts the distribution of *P* values (n = each 10,000 simulations) as a function of the number of the selected trials, which corresponds to the number of presynaptic calcium events used for the *P* value calculation. By thresholding the *P* values at 0.01, the rate of false-negative errors, i.e., the fraction that was >0.01, was plotted versus the number of presynaptic events (Fig. 4*A*, *right*). The false-negative error rate was inversely correlated with the presynaptic event count and the error rate was reduced to <5% when more than four events were considered. In other words, at least five calcium events were required to reach a 95% accuracy.

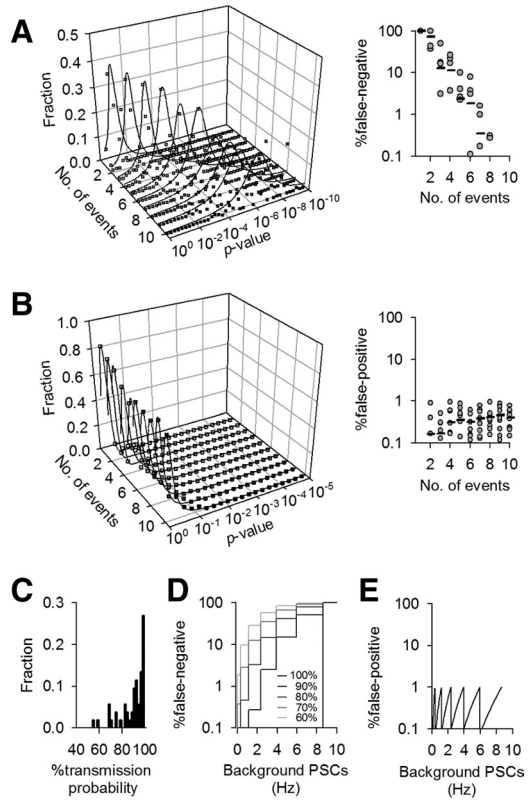

FIG. 4. Characterization of the detection power of ROTing. *A* and *B*: based on data sets of dual whole cell recordings from synaptically connected and unconnected neuron pairs, the false-negative rate [i.e., the probability that ROTing fails to detect real synaptic pairs (*A*)] and the false-positive rate [i.e., the probability that ROTing detects uncoupled pairs as synaptic pairs by error (*B*)] were estimated against the number of calcium events used for detection. The *left panels* show the distributions of *P* values given by synaptically connected (*A*) and unconnected (*B*) pairs. Sets of presynaptic spikes and PSCs were randomly collected to calculate the *P* values against the event counts ranging from one to 10. The lines are the best Gaussian fit. The *right plots* show the rates of false-negative (*A*) and false-positive (*B*) error detection at a *P* value threshold of 0.01. The dots and lines indicate individual data obtained from single neuron pairs and their average values, respectively. *C*: distribution of the transmission probability at unitary CA3–CA1 synapses. *D* and *E*: false-negative (*D*) and false-positive (*E*) error rates at different frequencies of background PSCs were simulated for synapses with different transmission probabilities ranging from 60 to 100%.

Similar analyses were applied to synaptically unconnected neurons ($n = 10$ pairs), to estimate the false-positive errors, i.e., errors in which unconnected pairs are judged as connected ones (Fig. 4*B*). In dual recordings from the uncoupled neurons, PSCs were recorded from one neuron, whereas the other neuron was fired by repetitive current injection. Based on these series of "apparent" success-or-failure trials, we calculated *P* values. In Fig. 4*B*, the *left panel* depicts the *P* value distribution and the *right panel* shows the rate of false-positive errors, i.e., the fraction that did not exceed 0.01, as a function of the number of presynaptic events (n = each 10,000 simulations). The false-positive error rate was always ≤1% and did not correlate with the event count. Mathematically, this result was expected because the *P* value was thresholded at 0.01, which theoretically corresponds to the false-positive error level.

Another factor that affects the accuracy of ROTing is the failure rate of synaptic transmission. Dual patch-clamp recordings were obtained from 52 CA3–CA1 monosynaptically connected pairs (35 slices). We searched them with ROTing and

calculated the transmission probability in our modified ACSF (30–100 trials for each pair). Although the median of the probability was 93%, some synapses exhibited much lower transmission efficiency (Fig. 4*C*). How do these unreliable synapses contribute to the false-negative error rate? We calculated the *P* value distribution and thereby the false-negative error rate by fixing the number of presynaptic events to seven and by changing the level of background PSCs in the range from 0 to 10 Hz (Fig. 4*D*). Given that the PSC frequency during ROTing was 2.6 ± 1.2 Hz in the modified ACSF, >10% of the synaptic connections will be missed when their transmission probabilities are <70%. On the other hand, similar analytical calculation revealed that the false-positive error rates were always <1%, regardless of background PSC levels (Fig. 4*E*).

Then we sought to estimate the detection power of ROTing under our experimental conditions. The background PSC frequency, synaptic transmission probability (Fig. 4*C*), and the frequency of glutamate-evoked calcium events were known from the previous experiments (Figs. 2*E* and 4*C*). Thus these parameters are weighted as a convolution integral onto the functions obtained in Fig. 4, *A* and *D*, and then the false-negative error rate is estimated to be roughly 4%. This means, in theory, that ROTing can detect about 96% presynaptic neurons tested in the focused region. On the other hand, based on Fig. 4, *B* and *E*, the false-positive error rates are estimated to be <1% and thus practically negligible.

Application of ROTing

ROTing is applicable for multiple patch-clamp recordings. In the following experiments, we considered only the presynaptic neurons that exhibited more than five calcium events (<5% false negative), which corresponded to about 75% of the stained cells in the imaged region. In Fig. 5, quadrant recordings were carried out from CA1 neurons and synaptic connections were searched in a CA3 network. In this case, the total recording time was 6.6 min and the puffing pipette was moved at a speed of 15 μm/s to cover the 300 × 520-μm^2 area. We identified 12 synaptic connections between these 4 CA1 neurons and 46 CA3 neurons and depicted their wiring map in Fig. 5*B*.

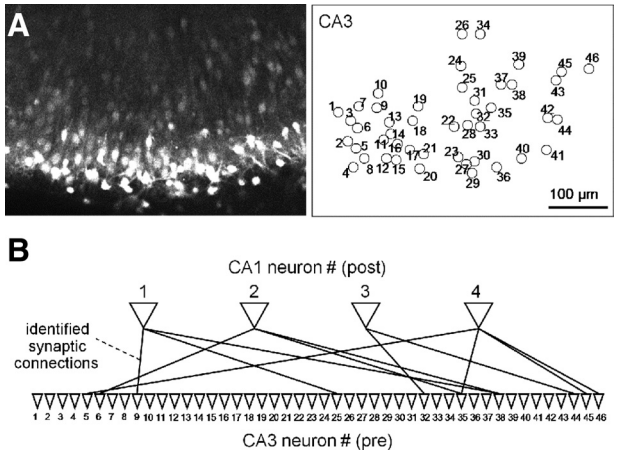

FIG. 5. Representative mapping for monosynaptic connections between hippocampal CA3 and CA1 regions. *A*: confocal image of the CA3 region (*left*), in which 46 neurons were searched for synaptic connectivity (*right*). *B*: ROTing-identified wiring patterns between 46 presynaptic CA3 neuron to 4 postsynaptic CA1 neurons. Triangles and lines indicate neurons and synaptic connections, respectively.

We next estimated how comprehensively ROTing can detect synaptic connections in real neuronal networks. The CA3-to-CA1 projection probability and its topographic pattern are known to depend on the relative positions of neurons (Amaral 1993) and this makes it difficult to precisely determine the ROTing power. Therefore we chose the CA3–CA3 recurrent connections. We carried out dual whole cell recordings from 94 randomly selected pairs of CA3 pyramidal cells in 20 slices. From these, 24 pairs (25.5%) were found to have monosynaptic connections. We next carried out ROTing in CA3 networks. In this assay, 10 neurons were patch-clamped in each slice (n = 3) and 27 ± 9 presynaptic candidate neurons were examined. Among these neurons we identified 63 ± 28 synaptic pairs. Thus the density of ROTing-probed synaptic connections was 24.8 ± 11.1%, which was almost equivalent to that found by random patch-clamp recordings.

By referring to the ROTing-defined wiring maps, we acquired targeted patch-clamp recordings from multiple neurons. Figure 6*A* shows triple whole cell recordings from a convergent circuit in which two presynaptic CA3 neurons projected to one common postsynaptic CA1 neuron. Figure 6*B* shows triple recordings from a divergent circuit in which one presynaptic CA3 neuron projected to two different postsynaptic CA1 neurons. ROTing also detects physically distant monosynaptic pairs. Figure 6*C* shows long-distance recordings from a presynaptic layer III neuron in the entorhinal cortex and a postsynaptic CA1 neuron. We also applied ROTing to search inhibitory presynaptic neurons by isolating inhibitory PSCs at a clamped voltage of 0 mV. Figure 6*D* shows triple recordings from a divergent circuit in which one inhibitory interneuron in the CA1 stratum radiatum projected to two CA1 pyramidal neurons.

Finally, we show that ROTing also works in acute slice preparations. In acute slices, however, some brain regions are hardly loaded with AM-dyes (Namiki et al. 2009) and thus the regions available for ROTing are limited. Here we chose granule cells in the dentate gyrus and searched mossy fiber synaptic connections between the dentate gyrus and the CA3 region. A CA3 pyramidal cell was whole cell recorded and the granule cell layer was trawled by glutamate puff (n = 3 slices), an example of which is shown in Fig. 7. We identified three synaptic connections among the patched neuron and 154 granule cells tested.

DISCUSSION

We have developed ROTing, a novel high-throughput method that searches synaptic contacts in local neuronal networks in situ. ROTing allows thoroughly unveiling the network connectivity among dozens of neurons in a relatively small network with >95% accuracy. With the aid of patch-clamp recordings targeted on the identified presynaptic candidates, we achieved simultaneous recordings from a microcircuit with multiple synaptic connections.

The ROTing technique is conceptually similar to ROPing developed by Aaron and Yuste (2006). The critical difference between ROTing and ROPing is the degree of the signal-to-noise ratio. Because ROPing is sensitive to background spon-

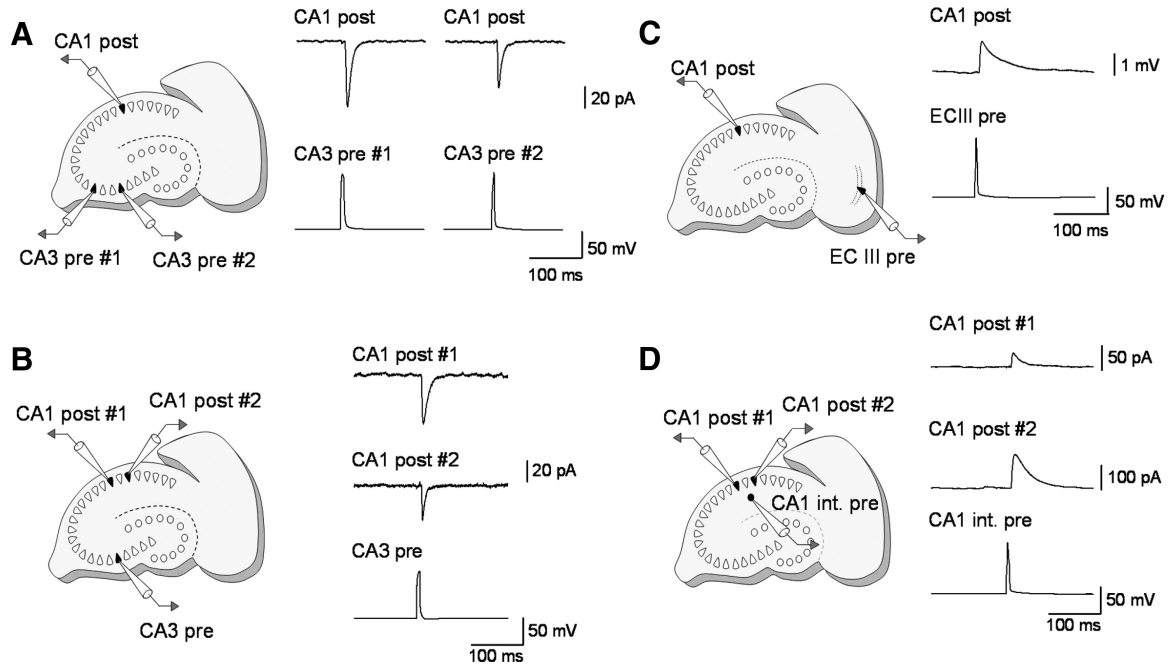

FIG. 6. Examples of multicell recordings from synaptically connected neuron pairs that were searched with ROTing. *A*: triple whole cell recordings from a convergent circuit in which 2 presynaptic CA3 neurons projected to one common postsynaptic CA1 neuron. *B*: triple whole cell recordings from a divergent circuit in which one presynaptic CA3 neurons projected to 2 different postsynaptic CA1 neurons. *C*: dual whole cell recordings from a distant monosynaptic pair between an entorhinal cortex layer III (EC III) neuron and a CA1 neuron. *D*: triple whole cell recordings from a divergent circuit in which one inhibitory interneuron in the CA1 stratum radiatum projected to 2 CA1 pyramidal neurons. During ROTing, the membrane voltages of the postsynaptic neuron was clamped at 0 mV.

taneous activity, it is very difficult, in practice, to determine a large number of synaptic connections. In our estimation, even if the searched synapses are quite reliable (100% transmission probability), the mean false-negative error rate of ROPing is about 62% after 30 min searching, considering a background PSC frequency of 63.7 Hz and the distribution of spontaneous activity rates in our normal ACSF ($n = 881$ neurons; Sasaki et al. 2007). This implies that lowering the background noise is indispensable to enhance the detection power. In addition, ROPing is not applicable to inactive presynaptic neurons; if the neurons did not exhibit any spontaneous calcium events during the probing period, one cannot calculate the P value. We resolved these two problems with the use of the modified ACSF and local activation of restricted neuron groups. The modified ACSF not only reduces the background PSC levels, but also increases the probability of synaptic release. Our computational simulation indicates that both contribute positively to the detection power of ROTing. As a result, we succeeded in reducing the false-negative error ratio of ROTing to about 4%. This estimation, however, was obtained based on the synaptic transmission probability for single presynaptic action potentials (Fig. 2*D*), but as shown in Fig. 4*A*, glutamate application often evoked bursts of action potentials, thus producing high synaptic release probability as a whole. We therefore speculate that the actual rate of false-negative errors is <4%.

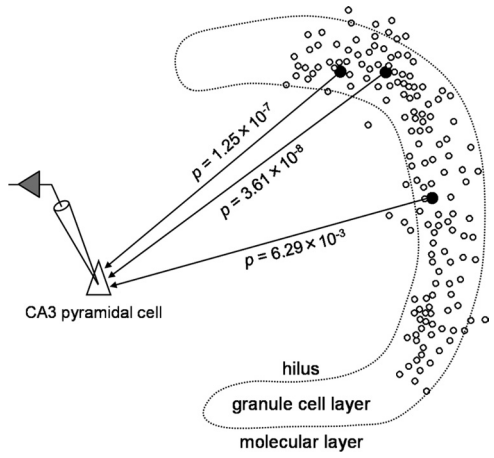

FIG. 7. Representative mapping for hippocampal mossy fiber connections between 154 dentate granule cells and a hippocampal CA3 cell in a mouse acute slice preparation. Among them, ROTing identified 3 putative synaptic pairs, which scored P values of <0.01 (lines).

It should be noted that, for physiological investigations of synaptic transmission and plasticity, the external solution needs to be switched to normal ASCF when targeted patch-clamp recordings were accomplished with ROTing because the elevated Ca^{2+} and Mg^{2+} could affect the basic properties of synapses.

There have been several attempts for searching synaptically connected neurons in electrophysiological studies. One is that a postsynaptic neuron is patch-clamped, like our method, and postsynaptic events are evoked by one-by-one activation of neurons in a presynaptic network with extracellular loose-seal stimulation (Debanne et al. 2008; Feldmeyer et al. 2005) and glutamate puff (Otsuka and Kawaguchi 2008), which also help to achieve simultaneous target recordings from connected pairs. Compared with these methods, ROTing enables higher-throughput mapping to rapidly identify multiple synaptic connections. Another procedure is to activate presynaptic neuron populations by puff application of high K^+ (140 mM) solution (Debanne et al. 2008; Mori et al. 2004). This also increases the success rate of finding monosynaptic connections up to about

10% at hippocampal mossy fiber synapses in slice cultures. The success rate remains relatively low, however, mainly because one cannot identify the exact neurons that are fired around the puff-pipette tip. To improve this, we combined these techniques with fMCI, which optically identifies presynaptically responsible sources and enables large-scale scanning of the network connectivity. Another promising strategy using fMCI has recently been developed, which searches synaptic connections with two-photon photolysis of caged glutamate (Nikolenko et al. 2007). This technique uses infrared light laser and is thus able to probe neurons deeply located in tissues and thereby perform three-dimensional mapping (Matsuzaki et al. 2008), whereas ROTing accesses only relatively shallow neurons (usually $\leq$50 μm in depth). However, our method is not technically complicated or expensive in terms of optical equipments and consumable supplies.

An alternative strategy is retrograde neuronal tracing with so-called transsynaptic virus, such as rabies and pseudorabies viruses, which can label cells projecting to the virus-infected neurons (Boldogkoi et al. 2009; Ohara et al. 2009; Wickersham et al. 2007). These methods identify a large number of functionally connected cells and are applicable to in vivo animals. However, they need the virus-infection process, which may not be suitable for electrophysiological recordings in terms of the cell health, and it also takes longer time, usually days, after virus infection to achieve sufficient transneuronal transports.

ROTing is potentially applicable to other brain regions and other types of nerve tissue preparations, so we believe that this technique is powerful and versatile for approaching the neuronal circuits at the single-synapse level. But we also have to note some technical limitations of ROTing. First, there would be some sampling biases. ROTing preferentially detects strong synapses with more reliable transmission because the detection power depends on the transmission probability (Fig. 4*D*). Second, the staining efficiency with AM-dyes varied depending on animal ages and brain regions (Ikegaya et al. 2005; Namiki et al. 2009). The maturity of neurons, in particular, is critical. In our experience, neurons in acute slices prepared from rodents at ages over postnatal day 17 are hardly loaded with AM-dyes. Genetically encoded fluorescent proteins that sensitively respond to spike-evoked rapid calcium increases have the potential to solve this problem (Miyawaki 2005; Wallance et al. 2008). Another limitation is that ROTing cannot be applied to neurons whose somatic calcium fluctuations are not linked to their action potential activity. For example, granule cells of the olfactory bulb in *Xenopus laevis* tadpoles are reported to show no stereotypical correlation between action potentials and calcium events (Lin et al. 2007) and thus care must be taken when interpreting ROTing data obtained from such atypical neurons.

ACKNOWLEDGMENTS

We thank R. Andersson (Karolinska Institute, Sweden) for critical comments on the manuscript.

GRANTS

This work was supported in part by Japan Society for Promotion of Science Grants-in-Aid for Scientific Research 18021008 and 17689004.

REFERENCES

Aaron G, Yuste R. Reverse optical probing (ROPING) of neocortical circuits. *Synapse* 60: 437–440, 2006.

Amaral DG. Emerging principles of intrinsic hippocampal organization. *Curr Opin Neurobiol* 3: 225–229, 1993.

Boldogkoi Z, Balint K, Awatramani GB, Balya D, Busskamp V, Viney TJ, Lagali PS, Duebel J, Pásti E, Tombácz D, Tóth JS, Takács IF, Scherf BG, Roska B. Genetically timed, activity-sensor and rainbow transsynaptic viral tools. *Nat Methods* 60: 127–130, 2009.

Bolshakov VY, Siegelbaum SA. Regulation of hippocampal transmitter release during development and long-term potentiation. *Science* 269: 1730–1734, 1995.

Debanne D, Boudkkazi S, Campanac E, Cudmore RH, Giraud P, Fronzaroli-Molinieres L, Carlier E, Caillard O. Paired-recordings from synaptically coupled cortical and hippocampal neurons in acute and cultured brain slices. *Nat Protoc* 3: 1559–1568, 2008.

Feldmeyer D, Roth A, Sakmann B. Monosynaptic connections between pairs of spiny stellate cells in layer 4 and pyramidal cells in layer 5A indicate that lemniscal and paralemniscal afferent pathways converge in the infragranular somatosensory cortex. *J Neurosci* 25: 3423–3431, 2005.

Ikegaya Y, Le Bon-Jego M, Yuste R. Large-scale imaging of cortical network activity with calcium indicators. *Neurosci Res* 52: 132–138, 2005.

Koyama R, Muramatsu R, Sasaki T, Kimura R, Ueyama C, Tamura M, Tamura N, Ichikawa J, Takahashi N, Usami A, Yamada MK, Matsuki N, Ikegaya Y. A low-cost method for brain slice cultures. *J Pharmacol Sci* 104: 191–194, 2007.

Le Bé BJ, Markram H. Spontaneous and evoked synaptic rewiring in the neonatal neocortex. *Proc Natl Acad Sci USA* 103: 13214–13219, 2006.

Lin BJ, Chen TW, Schild D. Cell type-specific relationships between spiking and $[Ca^{2+}]_i$ in neurons of the *Xenopus* tadpole olfactory bulb. *J Physiol* 582: 163–175, 2007.

Matsuzaki M, Ellis-Davies GC, Kasai H. Three-dimensional mapping of unitary synaptic connections by two-photon macro photolysis of caged glutamate. *J Neurophysiol* 99: 1535–1544, 2008.

Miyawaki A. Primer innovations in the imaging of brain functions using fluorescent proteins. *Neuron* 48: 189–199, 2005.

Mori M, Abegg MH, Gähwiler BH, Gerber U. A frequency-dependent switch from inhibition to excitation in a hippocampal unitary circuit. *Nature* 431: 453–456, 2004.

Namiki S, Sasaki T, Matsuski N, Ikegaya Y. Regional difference in stainability with calcium-sensitive acetoxymethyl-ester probes in mice brain slices. *Int J Neurosci* 119: 214–226, 2009.

Nikolenko V, Poskanzer KE, Yuste R. Two-photon photostimulation and imaging of neural circuits. *Nat Methods* 4: 943–950, 2007.

Ohara S, Inoue K, Yamada M, Yamawaki T, Koganezawa N, Tsutsui K, Witter MP, Iijima T. Dual transneuronal tracing in the rat entorhinal-hippocampal circuit by intracerebral injection of recombinant rabies virus vectors (Abstract). *Front Neuroanat* 3: 1, 2009.

Otsuka T, Kawaguchi Y. Firing-pattern-dependent specificity of cortical excitatory feed-forward subnetworks. *J Neurosci* 28: 11186–11195, 2008.

Pavlidis P, Madison DV. Synaptic transmission in pair recordings from CA3 pyramidal cells in organotypic culture. *J Neurophysiol* 81: 2787–2797, 1999.

Sanchez-Vives MV, McCormick DA. Cellular and network mechanisms of rhythmic recurrent activity in neocortex. *Nat Neurosci* 3: 1027–1034, 2000.

Sasaki T, Matsuki N, Ikegaya Y. Metastability of active CA3 networks. *J Neurosci* 27: 517–528, 2007.

Sasaki T, Takahashi N, Matsuki N, Ikegaya Y. Fast and accurate detection of action potentials from somatic calcium fluctuations. *J Neurophysiol* 100: 1668–1676, 2008.

Sayer RJ, Friedlander MJ, Redman SJ. The time course and amplitude of EPSPs evoked at synapses between pairs of CA3/CA1 neurons in the hippocampal slice. *J Neurosci* 10: 826–836, 1990.

Song S, Sjostrom PJ, Reigl M, Nelson S, Chklovskii DB. Highly nonrandom features of synaptic connectivity in local cortical circuits. *PLoS Biol* 3: e68, 2005.

Takahashi N, Sasaki T, Usami A, Matsuki N, Ikegaya Y. Watching neuronal circuit dynamics through functional multineuron calcium imaging (fMCI). *Neurosci Res* 58: 219–225, 2007.

Wallace DJ, Zum Alten Borgloh SM, Astori S, Yang Y, Bausen M, Kügler S, Palmer AE, Tsien RY, Sprengel R, Kerr JN, Denk W, Hasan MT. Single-spike detection in vitro and in vivo with a genetic calcium sensor. *Nat Methods* 5: 797–804, 2008.

Wickersham IR, Finke S, Conzelmann KK, Callaway EM. Retrograde neuronal tracing with a deletion-mutant rabies virus. *Nat Methods* 4: 47–49, 2007.